Vietnam Journal of Earth Sciences, 41(1), 1–9, Doi: 10.15625/0866-7187/41/1/13541

(VAST)

Vietnam Academy of Science and Technology

**Vietnam Journal of Earth Sciences**

http://www.vjs.ac.vn/index.php/jse

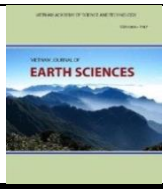


# Fluid characteristics from shallow magmatic environments: A contribution to danburite bearing Luc Yen pegmatites, northern Vietnam

Kurt Krenn[1*], Le Thi Thu Huong[1,2]

[1]*NAWI Graz Geocenter, University of Graz, Graz A-8010, Austria*
[2]*Zeichenakademie Hanau, Akademiestr. 52, D- 63450 Hanau, Germany*

Received 3 September 2018; Received in revised form 1 October 2018; Accepted 7 January 2019

ABSTRACT

Danburite as a member of the Luc Yen pegmatite mineral assemblage has been studied using fluid inclusion microthermometry and Raman spectroscopy. Data characterize well-preserved fluid inclusions which originate from primary large tubular inclusions as result of necking down. Same modifications underwent a second inclusion generation that evolved during healing of a later crack. Both generations of fluid inclusions show the same chemistry ($H_2O$-$CO_2$) characterizing 3-phase inclusions with additional solids (calcite, sassolite and danburite). Inclusions consist of pure $CO_2$ and $H_2O$ with additional NaCl ± KCl comprising a salinity of about 4.5 mass%. Internal fluid inclusion pressures as well as bulk inclusion densities have been calculated using the fermi diad split method of pure $CO_2$ at clathrate melting temperatures of the system and total homogenization temperatures, respectively. Mean internal pressures of ca. 4.5 MPa as well as a bulk density around 0.60 g/cm$^3$ represent a low-dense fluid with $XH_2O$~0.86 and $XCO_2$~0.14 in composition that was present during formation of danburite. Data characterize danburite as a late stage crystallization member of the pegmatite in a shallow magmatic environment.

*Keywords*: Pegmatites; danburite; fluid inclusions; necking down; Luc Yen.



## 1. Introduction and Geology

The Luc Yen mining area in northern Vietnam is a very productive gem district and one of the leading sources in South East Asia for ruby, sapphire, cobalt-blue spinel, watermelon tourmaline and apple-green orthoclase. Primary formations of ruby, sapphire and spinel in Luc Yen result from limestone metamorphoses, those of tourmaline and green orthoclase originate from granitic pegmatites. Recently, danburite ($CaB_2Si_2O_8$), a calcium borosilicate, was discovered in an alluvial deposit of ruby, sapphire, spinel and tourmaline at the base of the marble mountains. This danburite is notable for its high gem-quality by honey yellow color and excellent transparency. Genetically, danburite can be associated with granitic pegmatites, Ca-skarns or evaporites (Kurshakova, 1982; Anovitz and Grew, 1996). The area where danburite was found is located in a thick metasedimentary sequence of Cambrian age, composed of marble and overlying sillimanite-biotite-garnet schists (Fig. 1).

*Corresponding author, Email: kurt.krenn@uni-graz.at

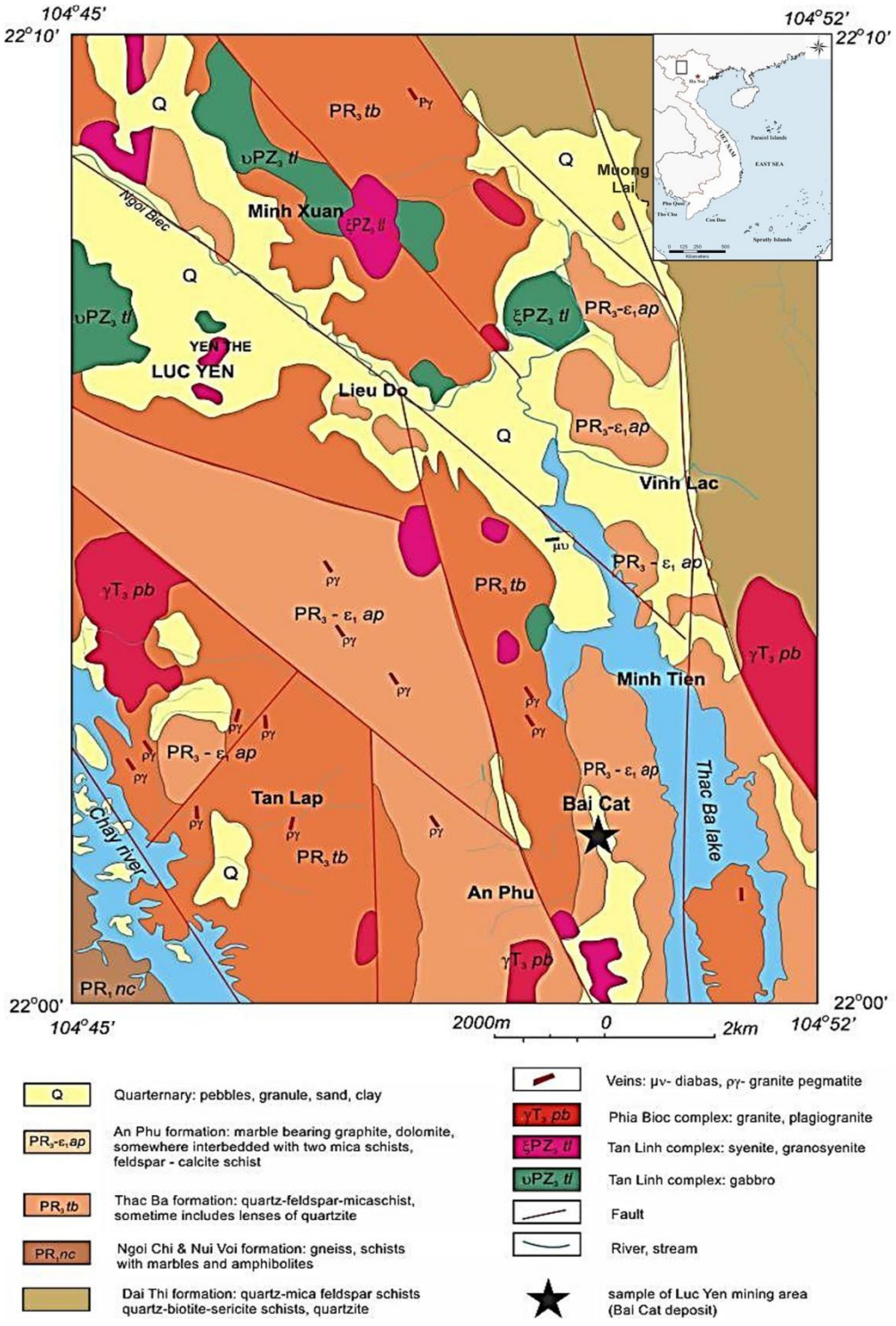


*Figure 1.* Geological map of Luc Yen mining district of northern Vietnam. Upper right corner shows regional position by a square. Studied pegmatite sample from the Bai Cat deposit is indicated by a black star at the lower right part of the map (after Chauvire et al., 2015)

The metamorphic units, bounded by left-lateral faults, are often intruded by granitoids and related pegmatites of Triassic age (Garnier et al., 2005). The marbles are mainly calcitic and interlayered with Al-, V-, and Cr-rich amphibolites (Chauviré et al., 2015). Two different types of marble occur: (1) ruby, brown amphibol and phlogopite bearing calcite marbles, and (2) spinel, green amphibole ± forsterite ± clinohumite ± chlorite bearing calcite-dolomite marbles. The pegmatites exhibit different dimensions and vary from some ten to some hundred meters in length and up to 10 meters in width. Two pegmatite bodies in the Luc Yen area, which were intruded in type 1 marble, have been mined as the sources for tourmaline, green orthoclase, mica and quartz but most of them are unexploited. Danburite crystals from the Bai Cat deposit are associated with ruby, sapphire, spinel and tourmaline and its location, known as the first site for yellow danburite, is close to the marble mountain chain. Ruby, sapphire and spinel are associated with metamorphites contrasting to tourmaline with pegmatite origin. Danburite occurs preferred near the contact zones between both rocks (marble and pegmatite lenses).

In the previous studies, Raman spectroscopy data of fluid inclusion and trace element investigations in alluvial yellow danburite crystals from the Luc Yen mining area indicate granitic pegmatite origins of the samples. Presented microthermometry data of fluid inclusions from this study give an overview of the occurring fluid during danburite host formation, a constituent of the Luc Yen pegmatites, and hence give further constraints for the formation conditions of these granitic pegmatites.

## 2. Material and Methods

One danburite crystal weighting 158 ct from Bai Cat alluvial deposit was used for this study (Fig. 2). Double polished thick sections (thickness ~0.15 mm) were prepared from this danburite sample in order to investigate fluid inclusions (FIs) using microthermometry combined with Raman microspectroscopy.

*Figure 2.* Yellow danburite crystal. Large-scale fluid inclusions can be already seen at macroscale. Vertical size of the danburite is ca. 5cm. Photo by L.T.-T. Huong

### *2.1. Microthermometry*

FIs were investigated using a Linkam THSMG600 heating and freezing stage with an operating range from -196°C to +600°C equipped with an Olympus 80x ULWD objective at the NAWI-Graz Geocenter, University of Graz. The Synthetic Fluid Inclusion Reference Set (Bubbles Inc., Blacksburg,VA, USA) was used for stage calibration. Temperature measurements are reproducible to within 0.2°C at a heating rate of 0.1°C $min^{-1}$. Depending on the compositional system for any given FI, the following values are documented (L: liquid phase; V: vapor phase): $T_e$(Ice) eutectic temperature or apparent eutectic temperature

of ice (e.g. IceV → IceLV); $T_e$ was used to identify the saline aqueous fluid system after Davis et al. (1990) and Goldstein and Reynolds (1994); $T_m$(Ice) final melting temperature of ice (IceLV → LV); final melting temperature of $CO_2$ given as $T_m(CO_2)$ and $T_m$(Cla) defines final melting of the $CO_2$ clathrate phase. The heating-freezing stage was also mounted on the Raman microspectrometer HR800 to obtain $CO_2$ densities at $T_m$(Cla) by using the Fermi diad peak splitting method [Fermi doublet (Δ)] and density equation (l) after Fall et al. (2011). Using Δ directly at $T_m$(Cla) enables an estimation on the pressure of a given fluid inclusion assemblage ($P_{FI}$) because $P_{FI}$ and $T_m$(Cla) intersect on the salinity dependent clathrate stability boundary. The freezing point depression of clathrate in a mixture of NaCl, KCl, HCl, and <10% $CaCl_2$ and $FeCl_2$ in vapor inclusions will behave almost identically to pure NaCl (Tattitch et al., 2015). Salinities of the aqueous fluid phase have been calculated using freezing point depression of ice after Bodnar (1993) but also using software CLATHRATES Q2 (Bakker, 1997). As the last step, total homogenization temperatures $T_h$(total) (LV → L and/or V) were measured to obtain minimum conditions for the formation of homogeneous trapped FIs by crossing the isochores with the high temperature boundary of the $H_2O$-$CO_2$ immiscibility field (i.e. bubble and dew curves for high and low pressures, respectively after Diamond 2003). Because of a wide range in increased $T_h$(total) values of all inclusions as result from post-entrapment modifications (i.e. necking down), *V-x* diagram after Bakker and Diamond (2000) was not applied. Fluid inclusion microthermometry data are given in Table 1.

*Table 1.* Microthermometry data from FIs in danburite host

| Type | Texture | n | Size (μm) | phases | $T_m(CO_2)$ (°C) | $T_m$(Cla) (°C) | $T_h(CO_2)$ (°C) | $T_e$(Ice) (°C) | $T_m$(Ice) (°C) | $T_h$(total) (°C) | Salinity (mass%) | Fermi split Δ | Bulk density (g/cm$^3$) | Chemistry |
|---|---|---|---|---|---|---|---|---|---|---|---|---|---|---|
| Type A | Primary necked | 18 | >150 to 20 | L,L,V,S | -56.6 to -56.8 | 8.3 to 9.8 | 19.0 to 25.8 | -23.5 to -21.2 | -5.6 to -3.1 | 331.7 to 346.0 | 4.44 | 102.72 to 103.25 | 0.59 to 0.62 | $CO_2$-$H_2O$-NaCl ± KCl |
| Type B | Pseudo-secondary necked | 22 | <100 | L,L,V, S | -56.7 | 9.1 to 9.5 | 23.3 to 27.1 | -23.7 to -24.1 | -2.9 to -3.5 | 293.3 to 375.9 | n.c. | 102.54 to 103.92 | n.c. | $CO_2$-$H_2O$-NaCl ± KCl |

*Note*: abbreviation n (number of measured FIs); n.c. (not calculated); L (liquid); V (vapor); S (solid)

### *2.2. Raman Spectroscopy*

The ability of Raman spectroscopy to acquire data from aqueous and/or carbonic solutions together with the high spatial resolution of the Raman microprobe make it well suited for non-destructive analysis of gas, liquid and solid phases in small (≥ 5 μm) FIs. Raman spectra of FIs were established in confocal mode using a HORIBA Jobin Yvon LabRam HR800 micro-spectrometer equipped with an Olympus BX41 optical microscope and a Si-based CCD (charged-coupled device) detector at the NAWI-Graz Geocenter, University of Graz. The instrumentation uses a 100mW Nd-YAG laser (532 nm emission), a grating of 1800 grooves/mm, and a slit width of 100 μm. The spectral acquisition time was set to 20 seconds for all measurements in the range from 150 to 4000 cm$^{-1}$.

## 3. Results

FIs in danburite can be separated by their textural appearance in two major types. Early multi-phase, partly tube-like inclusions (type A) arranged along crystallographic axes of the host mineral and/or along their cleavage

planes and later multi-phase rounded FIs (type B), which show crosscutting relationships to type A (Figs. 3a/b). Due to post entrapment modifications, type A FIs originate from large-scale fluid-filled tubes that have been separated into elongated FIs with variable phase volume fractions as result of necking down in the inclusions. The same modification process affected type B inclusions, which evolved from necking down during crack healing (Figs. 3c/d). Based on intergranular cracks, type B FIs characterize pseudo-secondary inclusions (Roedder, 1984). Both types of FIs show different phase ratios and different phase assemblages. Due to necking down, some inclusions are connected with other bubble-free inclusions by thin tubes (Fig. 3e). Petrographic observations at room temperatures show that both FI types consist of aqueous liquid ($H_2O^L$) containing a carbonic liquid bubble ($CO_2^L$) and a carbonic vapor bubble ($CO_2^V$) (Fig. 3f). The various amounts of solid phases, suggested as daughter crystals, which became trapped during growth of the danburite host crystal, are identified as calcite, sassolite and danburite (Figs. 4a/b).

### *3.1. Fluid inclusion type A*

Type A inclusions have high variations in size between >150 and 20µm. Inclusions appear as three phase inclusions of $H_2O^L$-$CO_2^L$-$CO_2^V$ with additional daughter minerals danburite, sassolite and calcite (Figs. 3f-h). However, $CO_2^L$ becomes more visible during cooling when the large $CO_2^V$ decreases in size, finally compressed by the carbonic ice below -85°C. Last melting temperatures $T_m(CO_2)$ lie between -56.6 and -56.8°C, indicative for pure $CO_2$. Pure $CO_2$ gas phase is supported by Raman spectra, which show no peaks for additional phases like e.g. $CH_4$, $H_2S$ or $N_2$ (Fig. 4c). $H_2O^L$ shows $T_e$(ice) between -23.5 and -21.2°C indicative for a $H_2O$-NaCl±KCl fluid system. $T_m$(ice) between -5.6 and -3.1°C points to salinities between 8.7 and 5.1 mass% NaCl after Bodnar (1993). These salinity values, however, are considered as showing large uncertainties in the low-pressure range of FIs. According to arguments after Fall et al. (2011), this is due to the formation of a hydrate that incorporates $H_2O$ into the structure and salinities estimated from $T_m$(ice) should be higher compared to their actual salinities.

Fermi doublets (Δ) of pure $CO_2$ gas inclusions between 102.72 and 103.25 $cm^{-1}$ at $T_m$(Cla) between 8.3 and 9.8°C were determined resulting into densities between 0.03 and 0.24 $g/cm^3$, respectively, by using equation (1) in Fall et al. (2011) (Figs. 4d, 5a). Densities confirm the upper limit of calculated densities from 0.18 to 0.25 $g/cm^3$ by using EoS after Duan et al. (1996) in software package Q2 (Bakker, 1997) and average $T_m$(Cla) of 9.0°C. Calculated salinities are about 4.44 mass% NaCl. Calculated salinity crossed with $T_m$(Cla) of 9.0°C, results in fluid inclusion pressures ($P_{FI}$) at the clathrate stability boundary around 4.4 MPa (Fig. 6).

Isochores intersect the $CO_2$ boiling curve at $T_h(CO_2)$ between 19.0 and 25.8°C by considering the consistent homogenization trends of the carbonic vapor bubble into the vapor phase above clathrate stability (stars in Fig. 6). Isochore field corresponds to calculated densities for $CO_2$ in equilibrium with the aqueous solution. However, isochore gradients were not calculated for this low-temperature range. Further heating of coexisting $H_2O^L$+$CO_2^V$ inclusions results into total homogenization of $CO_2^V$ into the $H_2O^L$ phase at $T_h$(total) between 331.7 and 346.0°C. Using EoS after Duan et al. (1996) a pressure dominated supercritical fluid with $XH_2O$~0.86 and $XCO_2$~0.14 with a bulk density range from 0.59 to 0.62 $g/cm^3$ was calculated. It represents an approximation for

the homogeneous liquid fluid that entrapped during danburite formation.

### *3.1. Fluid inclusion type B*

Type B consists of smaller FIs <100µm that are clearly related to a crosscutting intragranular crack (Figs. 3c/d). Their orientation suggests healing from the original fluid-filled micro-cracks. Inclusions consist of same components and daughter minerals like type A but show clear higher variabilities in liquid/vapor phase ratios (Fig. 3d). This points to incomplete crack healing dominated by necking down of a large fluid-filled network (Roedder, 1984).

Type B inclusions are characterized by 3-phase $H_2O^L$-$CO_2^L$-$CO_2^V$ FIs with additional solids identified as calcite and sassolite. $T_m(CO_2)$ is constant at –56.7°C and the aqueous solution is explained by $T_e$(ice) at –23.9°C and $T_m$(Ice) around –3.2°C. Together with clathrate melting temperatures $T_m$(Cla) around 9.3°C the same fluid chemistry like type A can be proposed for type B FIs. However, total homogenization temperatures [$T_h$(total)] to the liquid show a wider range in temperatures between 293.3°C and 375.9°C of about 95% of the inclusions. A small number of ca. 5% homogenizes to the liquid between 179.2 and 215.9°C. The high range in $T_h$(total) into liquid as well as various partial homogenization trends of the $CO_2$ gas bubble into liquid but also vapor [$T_h(CO_2)$] between 23.3 and 27.1°C, supports the dominance of necking-down of larger inclusions during crack healing.

Densities derived from Fermi doublets (Δ) between 102.54 and 103.92 $cm^{-1}$ at $T_m$(Cla) were determined and result into densities between 0.04 and 0.54 $g/cm^3$, respectively, by using equation (1) in Fall et al. (2011). Higher densities are linked with partial homogenization of the $CO_2$ gas bubble into liquid above 0.46 $g/m^3$ (stripped horizontal line in Fig. 5a).

## 4. Discussions and Conclusions

FI textures and microthermometry indicate that type A and B inclusions of comparable chemistry evolved from former large tubular inclusions and crack-bounded fluid networks, respectively, both modified by necking down. However, tubular entrapped earlier than crack networks but comparable ranges in $T_h$(total) suggest that necking down must have occurred after entrapment of both types. It is also shown that smaller-scale type B have been more affected than large-scale type A inclusions. However, density changes due to post entrapment modification resulted in the high range in densities between 102.72 and 103.25 $cm^{-1}$, obtained by $CO_2$ vapor phases in type A inclusions, that lie between 1.5 and 6.5 MPa, respectively (Fig. 5b). Densities in type B inclusions fit the trend by a more extended range in $T_h$(total) and Fermi diad for the $CO_2$ vapor and liquid phases (Fig. 5a). However using average $T_m$(Cla) of 9.0°C, internal fluid pressures ($P_{FI}$) of about 4.4 MPa seem to be therefore a well resulting mean pressure value, representative for earliest type A inclusions (Fig. 6). Because necking down characterizes almost an isothermal process near trapping temperatures (Roedder, 1984), $T_h$(total) of type A FIs should be only little below trapping temperatures of these inclusions, indicating danburite as a very late mineral phase that formed during cooling of the pegmatite system. $CO_2$ densities below 0.3 $g/cm^3$ as well as relatively low bulk densities from 0.59 to 0.62 $g/cm^3$ support that danburite, as a late crystallized pegmatite mineral constituent, holds important indications that the Luc Yen pegmatite mining area evolved in a shallow intrusive magmatic environment.

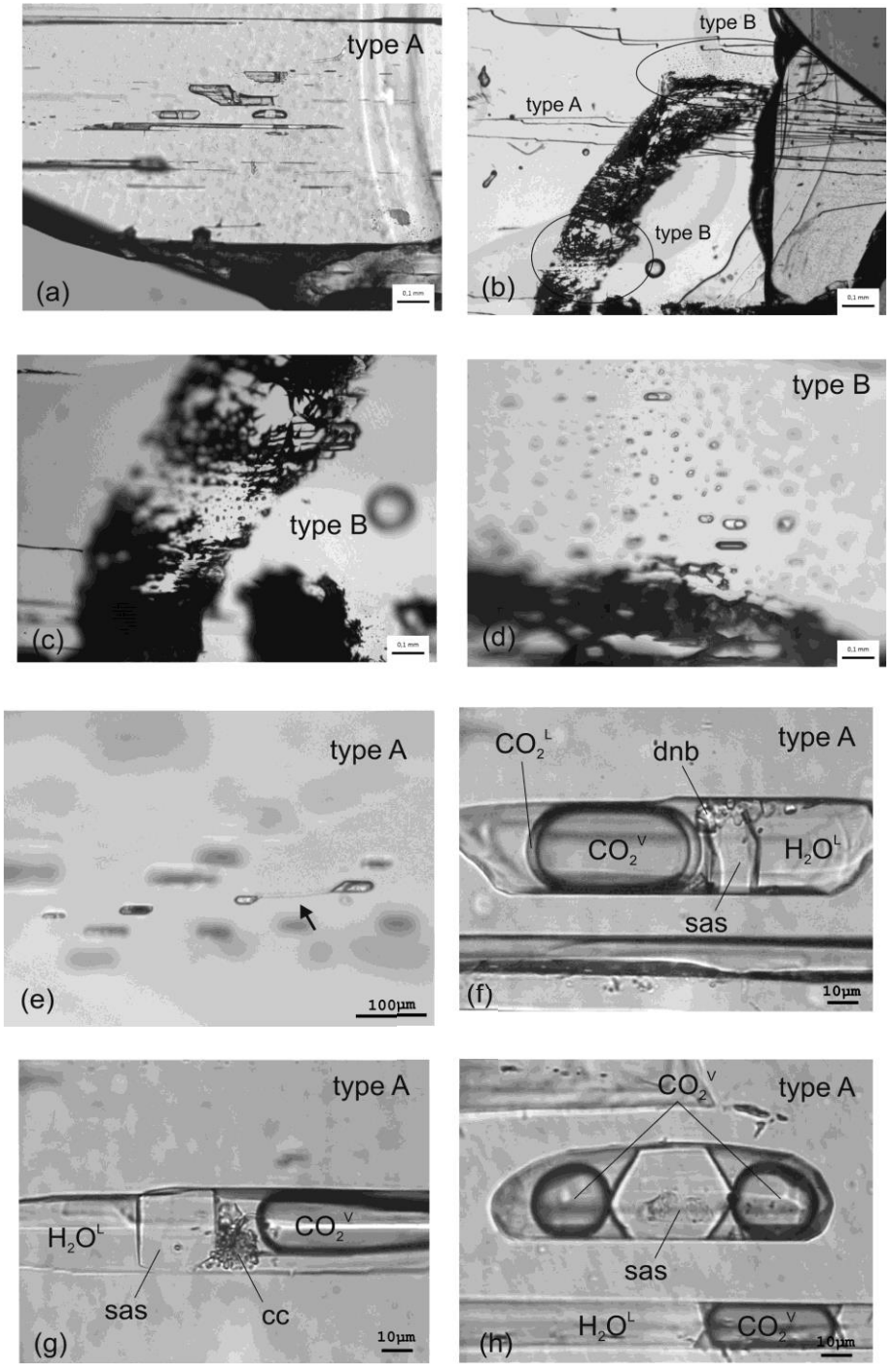


*Figure 3*. Microphotographs of studied FIs. (a): Polyphase type A FIs arranged parallel to crystallographic growth direction as large-scale tube-like inclusions. (b): Micro-crack cutting type A tubular inclusions. Crack is locally healed by necking down of type B FIs (black ellipsoids). (c) & (d): Detail of type B FIs. Note variable $H_2O$ and $CO_2$ phase volume fractions, indicative for necking-down of the inclusions. (e): Necking down in type A FIs shown by connection between the inclusions by thin tubes (arrow). (f) - (h): Detail of large-scale type A FIs including volatile phases and solid minerals (abbreviations: dnb-danburite; sas-sassolite; cc-calcite). See text for further explanations

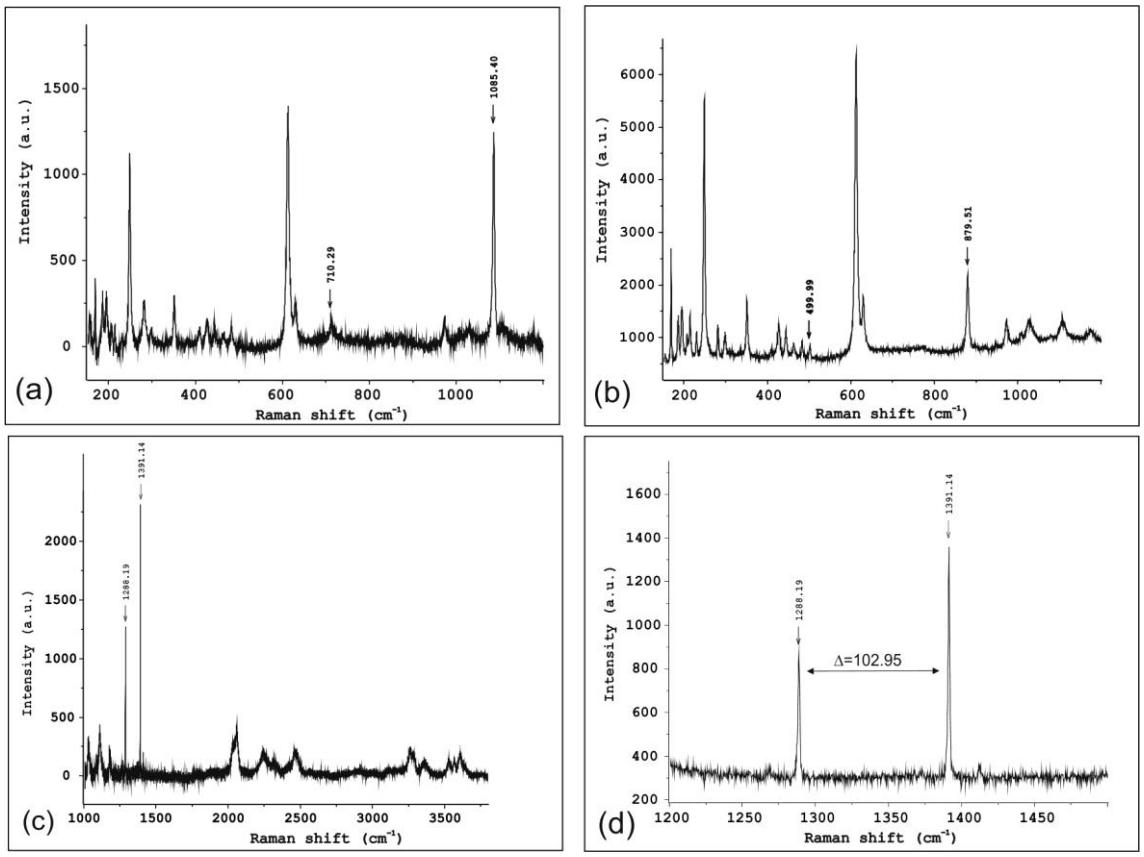


*Figure 4.* Representative Raman spectra of: mineral inclusions (a) calcite and (b) sassolite; (c) pure $CO_2$ and (d) $CO_2$ fermi diad split Δ at $T_m$(Cla). Corresponding peaks for the specific phases are numbered. Remaining peaks are related to host mineral danburite

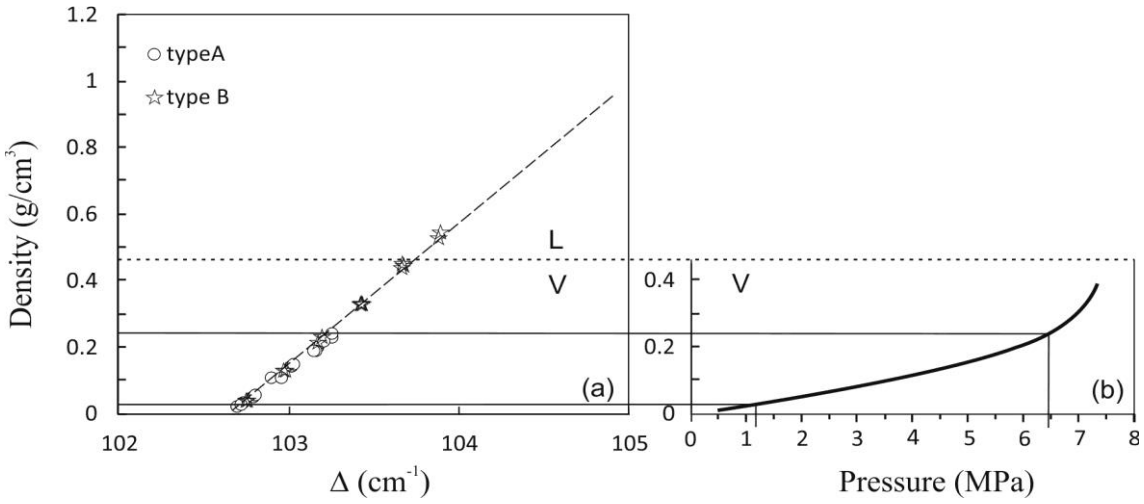


*Figure 5.* (a) Splitting of the fermi diad (Δ) of pure $CO_2$ as a function of density for type A and type B inclusions. Stripped line indicates transition of $CO_2$ gas bubble from vapor (V) into liquid (L) at 0.46 g/m$^3$. (b) $CO_2$ density as a function of pressure. Fit line and diagrams after Fall et al. (2011)

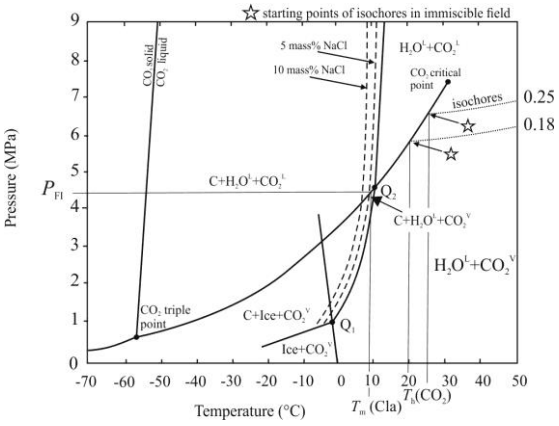


*Figure 6*. Clathrate stability diagram for low-pressure $H_2O$-$CO_2$ clathrates applied to type A inclusions after Fall et al. (2011). Dashed lines represent the $CO_2$ clathrate stability curves for clathrate in equilibrium with aqueous solutions of 10 and 5 mass% NaCl. Clathrate is stable at higher temperatures than ice. The isochores intersect the $CO_2$ critical curve (location of stars) at temperatures above clathrate stability defined by $T_h(CO_2)$. Mean internal fluid pressure $P_{FI}$ value of about 4.4 MPa results from crossing $T_m$(Cla) at 9°C with clathrate stability curve of ca. 4.4 mass% NaCl in aqueous solution. For further interpretation of the diagram the reader is referred to Fall et al. (2011) and Tattich et al. (2015)

## Acknowledgements

The authors are grateful to the ASEAN-European Academic University Network, the Austrian Federal Ministry of Science, Research and Economy, and the Austrian Agency for International Cooperation in Education and Research for financial support. Two anonymous reviewer and the journal editor are thanked for their suggestions which improved the manuscript.

## References

Anovitz L.M., Grew E.S., 1996. Mineralogy, petrology and geochemistry of boron: An introduction. In L.M. Anovitz and E.S. Grew, Eds., Boron: Mineralogy, Petrology, and Geochemistry, Reviews in Mineralogy, Mineralogical Society of America, Washington DC, USA, 33, 1–40.

Bakker R.J., 1997. Clathrates: computer programs to calculate fluid inclusion V–X properties using clathrate melting temperatures. Computer & Geosciences, 23, 1–18.

Bakker R.J., Diamond L.W., 2000. Determination of the composition and molar volume of $H_2O$–$CO_2$ fluid inclusions by microthermometry. Geochimica et Cosmochimica Acta, 64, 1753–1764.

Bodnar R.J., 1993. Revised equation and table for determining the freezing point depression of H2O-NaCl solutions. Geochimica et Cosmochimica Acta, 57, 683–684.

Chauviré B., Rondeau B., Fritsch E., Ressigeac P., Devidal J.-L., 2015. Blue spinel from the Luc Yen District of Vietnam. Gems & Gemology, 51(1), 2–17.

Diamond L., 2003. Glossary: Terms and symbols used in fluid inclusion studies, In: Samson, I., Anderson, A., Marshall, D. (Eds.), Fluid Inclusions: Analysis and Interpretation. Mineralogical Association of Canada Short Course Series, 32, 365–374.

Duan Z., Møller N., Weare J.H., 1996. A general equation of state for supercritical fluid mixtures and molecular dynamics simulation of mixture PVTX properties. Geochimica et Cosmochimica Acta, 60, 1209–1216.

Davis D.W., Lowenstein T.K., Spencer R.J., 1990. Melting behavior of fluid inclusions in laboratory-grown halite crystals in the systems NaCl-$H_2O$, NaCl-KCl-$H_2O$, NaCl-$MgC1_2$-$H_2O$, and NaCl-$CaCl_2$-$H_2O$. Geochimica et Cosmochimica Acta, 54, 591–601.

Fall A., Tattrich B., Bodnar R.J., 2011. Combined microthermometric and Raman spectroscopic technique to determine the salinity of $H_2O$-$CO_2$-NaCl fluid inclusions based on clathrate melting. Geochimica et Cosmochimica Acta, 75, 951–964.

Garnier V., Ohnenstetter D., Giuliani G., Maluski H., Deloule E., Phan Trong T., Pham Van L., Hoang Quang V., 2005. Age and significance of ruby bearing marble from the Red River shear zone, northern Vietnam. Canadian Mineralogist, 43(4), 1315–1329.

Goldstein R.H., Reynolds T.J., 1994. Systematics of fluid inclusions in diagenetic minerals. SEPM Short Course 31.

Kurshakova L.D., 1982. Temperature regime and geochemical conditions of formation of danburite. International Geology Review, 24(3), 367–371.

Roedder E., 1984. Fluid Inclusions. Reviews in Mineralogy, 12, 646.

Tattitch B.C., Candela P.A., Piccoli P.M., Bodnar R.J., 2015. Copper partitioning between felsic melt and $H_2O$-$CO_2$ bearing saline fluids. Geochim.